AFRL-RD-PS-
TP-2009-1022

INITIAL RESULTS FROM IMPLEMENTING AND TESTING A MEMS ADAPTIVE OPTICS SYSTEM: POST PRINT

Julie Smith, et. al

Boeing LTS Inc.
6200 Uptown Blvd Suite 240
Albuquerque, NM 87110-4142

1 July 2009

Technical Paper

AIR FORCE RESEARCH LABORATORY
Directed Energy Directorate
3550 Aberdeen Ave SE
AIR FORCE MATERIEL COMMAND
KIRTLAND AIR FORCE BASE, NM 87117-5776

REPORT DOCUMENTATION PAGE

Form Approved
OMB No. 0704-0188

1. REPORT DATE *(DD-MM-YYYY)*	2. REPORT TYPE	3. DATES COVERED *(From - To)*
01-07-2009	Technical Paper	Jan 1, 2006 -Jul 1, 2009

4. TITLE AND SUBTITLE

Initial results for implementing and testing a MEMS adaptive optics systems: post print

5a. CONTRACT NUMBER
FA9451-05-C-0257 S020AGS DF297711

5b. GRANT NUMBER

5c. PROGRAM ELEMENT NUMBER
63605F

6. AUTHOR(S)

Julie Smith, Darryl Sanchez, Denis Oesch, Nathan Engstrom, Loretta Arguello, Carolyn Tewksbury-Christle, Kevin Vitayaudom, Patrick Kelly

5d. PROJECT NUMBER
DIRECT CITE

5e. TASK NUMBER
DIRECT CITE

5f. WORK UNIT NUMBER
DIRECT CITE

7. PERFORMING ORGANIZATION NAME(S) AND ADDRESS(ES)
Boeing LTS Inc.
6200 Uptown Blvd Suite 240
Albuquerque, NM 87110

8. PERFORMING ORGANIZATION REPORT NUMBER

9. SPONSORING / MONITORING AGENCY NAME(S) AND ADDRESS(ES)

Air Force Research Laboratory
3550 Aberdeen Ave SE
Kirtland AFB NM 87117-5776

10. SPONSOR/MONITOR'S ACRONYM(S)
AFRL/RDSEW

11. SPONSOR/MONITOR'S REPORT NUMBER(S)
AFRL-RD-PS-TP-2009-1022

12. DISTRIBUTION / AVAILABILITY STATEMENT

Approved for public release

13. SUPPLEMENTARY NOTES
Accepted for publication in the SPIE Conference Proceedings; San Diego, CA; July 6, 2009. 377AWB-2009-0921; July 14, 2009. "Government Purpose Rights" PA approval 377ABW-2009-0921 dtd 14 Jul 09

14. ABSTRACT
This paper is the 3rd in a series of papers discussing characterization of a Micro-Electrical-Mechanical-System (MEMS) deformable mirror in adaptive optics. Here we present a comparison between a conventional adaptive optics system using a Xinetics continuous face sheet deformable mirror with that of segmented MEMS deformable mirror. We intentionally designed the optical layout to mimic that of a conventional adaptive optics system. We present this initial optical layout for the MEMS adaptive optics system and discuses problems incurred with implementing such a layout; also presented is an enhanced optical layout that partially addresses these problems. Closed loop Strehl highlighting the two systems will be shown for each case as well. Finally the performances of both conventional adaptive optics and the MEMS adaptive optics system is presented for a range of adaptive optics parameters pertinent to astronomical adaptive optics leading to a discussion of the possible implication of introducing a MEMS adaptive optics system into the science community.

15. SUBJECT TERMS
Adaptive Optics, MEMS, Deformable Mirror

16. SECURITY CLASSIFICATION OF:			17. LIMITATION OF ABSTRACT	18. NUMBER OF PAGES	19a. NAME OF RESPONSIBLE PERSON
					Dan Devany
a. REPORT	b. ABSTRACT	c. THIS PAGE			19b. TELEPHONE NUMBER *(include area code)*
Unclassified	Unclassified	Unclassified	SAR	14	505-853-7530

Standard Form 298 (Rev. 8-98)
Prescribed by ANSI Std. 239.18

Initial results from implementing and testing a MEMS adaptive optics system

Julie C. Smith[a], Darryl J. Sanchez[a], Denis W. Oesch[a], Nathan Engstrom[a], Loretta Arguello[a], Carolyn M.Tewksbury-Christle[a], Kevin P. Vitayaudom[a], Patrick R. Kelly[a]
[a]Starfire Optical Range, Air Force Research Labs, Kirtland Air Force Base, New Mexico, USA

ABSTRACT

This paper is the 3rd in a series of papers discussing characterization of a Micro-Electrical-Mechanical-System (MEMS) deformable mirror in adaptive optics. Here we present a comparison between a conventional adaptive optics system using a Xinetics continuous face sheet deformable mirror with that of segmented MEMS deformable mirror. We intentionally designed the optical layout to mimic that of a conventional adaptive optics system. We present this initial optical layout for the MEMS adaptive optics system and discuss problems incurred with implementing such a layout; also presented is an enhanced optical layout that partially addresses these problems. Closed loop Strehl highlighting the two systems will be shown for each case as well. Finally the performances of both conventional adaptive optics and the MEMS adaptive optics system is presented for a range of adaptive optics parameters pertinent to astronomical adaptive optics leading to a discussion of the possible implication of introducing a MEMS adaptive optics system into the science community.

Keywords: adaptive optics, MEMS, deformable mirror

1. INTRODUCTION AND BACKGROUND

There is a high demand for producing next generation adaptive optics (AO) systems for use on telescopes in the astronomical community. For centuries astronomers have been plagued by the deleterious effects of the atmosphere on their ground based images. Images formed on the focal plane of a telescope suffer from higher order phase distortion and an overall tilt on wavefronts, caused by atmospheric turbulence, thus forming an aberrated image at the location of the camera.

AO has greatly enhanced the performance of ground based telescopes allowing for new discoveries and more productive research. The use of AO on ground based telescopes allows astronomers to achieve diffraction-limited imaging and hence high quality science. AO systems consist of a wavefront sensor (WFS) to detect the optical disturbance, a deformable mirror (DM) to correct for the optical disturbance, and a control computer to monitor the sensor information for the DM[(1)]. These AO systems work to continuously remove higher order distortions to stabilize the position of astronomical images by removing the overall tilt [(2)]. These are dynamical optical systems that simultaneously relay the image to the science camera while removing the higher order aberrations with the deformable mirror and tilt aberrations with a fast steering mirror (FSM) leaving only a minor amount of the residual error in the wave front [(2)]. Conventionally, the components of an AO system are housed in a room beneath the telescope called a Coudé room where the fitting of the large components will not interfere with the balance of the telescope, nor heat the air in the optical path creating additional distortion. New, smaller AO systems are proposed for mounting on a gimbal directly on the telescope. The MEMS devices we study here are a potential candidate for possible new mounting schemes.

To understand how the DM's are performing as a function of time we look at Strehl versus frame number of a given data set. Strehl is a basic metric of the performance of an AO system and is a ratio of the observed peak intensity at the image plane compared to the maximum theoretical peak intensity of a diffraction limited system. Astronomers frequently use Strehl as the metric of choice to determine the performance of their AO system because Strehl ratios are directly tied to image sharpness. Higher Strehl ratios allow for more resolved images thus increasing the chance of new discoveries.

Currently AO systems excel in regimes characterized by low scintillation. Scintillation is related to atmospheric strength and length of the propagation after encountering turbulence. Typically this is the regime astronomers work in, i.e. small zenith angles. Increasing the zenith angle increases scintillation because the amount of atmosphere the wave travels through increases. Current AO technology performs well in weak and moderate turbulence. The conventional

Advanced Wavefront Control: Methods, Devices, and Applications VII, edited by Richard A. Carreras, Troy A. Rhoadarmer, David C. Dayton, Proc. of SPIE Vol. 7466, 74660F · © 2009 SPIE · CCC code: 0277-786X/09/$18 · doi: 10.1117/12.829941

technology used to correct this disturbance uses a single continuous face sheet DM that is conjugate to both the wavefront sensor (WFS) and the pupil (a virtual aperture that defines the area that accepts light). The WFS is a Shack-Hartmann type with the phase calculated using a least square reconstructor.

One limitation of AO is fitting error. Fitting error results from the DM not being able to exactly match the functional form of the turbulence. Fitting error is given by

$$\sigma^2 = \mu\left(\frac{d}{r_0}\right)^{5/3}, \quad (1)$$

where d is the sample spacing of actuators (mapped to the telescope aperture plane), μ is a fitting parameter related to the stiffness of a DM, and r_0 is the Fried's coherence length. This expression takes into account the coupling between the actuators.

This paper focuses on the introduction of a new type of deformable mirror for use in AO systems. We compare performance of a traditional continuous face sheet DM with that of a segmented Micro-Electro-Mechanical System (MEMS) DM. MEMS is the integration of mechanical elements, sensors, actuators and electronics on a common silicon substrate through microfabrication technology [3]. MEMS brings together silicon-based mircoelectronics with micromachining technology, making possible the realization of complete systems on a chip [3].

MEMS DM's can be segmented and it has been shown that as r_0 decreases, the fitting error increases for both a segmented and continuous face sheet DM. A segmented DM does not have coupling between actuators so it can better fit turbulence conditions with higher scintillation as compared to a continuous DM.

This research will compare the performances of the two types of DM's under turbulence conditions with various coherence lengths and scintillation. Therefore each correction system will be evaluated in how well it can mitigate the turbulence. For this research we compare the two DM's by looking at the Strehl ratio versus time and the scintillation of each turbulence condition.

Section 2 will detail the experimental setup while section 3 will discuss the control system. Results and discussion will be presented in section 4.

2. EXPERIMENTAL SETUP

The Atmospheric Simulation and Adaptive-optics Laboratory Testbed (ASALT) is well equipped to test multiple DM's under the same turbulence conditions. The ASALT lab has a single AO system containing both a Boston MicroMachines MEMS DM as well as a Xinetics DM.

2.1 Optical set-up

The ASALT lab uses an Atmospheric Turbulence Simulator (ATS) to simulate a two layer atmosphere with Kolmogorov turbulence [4]. The ATS consists of two phase screens generated by LexiTek used to simulate low and high altitudes. The ATS allows for well controlled, repeatable atmospheric conditions by controlling r_0 (Fried's coherence length), Rytov number (log-amplitude variance), and Greenwood frequency which is a measure of the characteristic frequency of the tilt of the atmosphere.

The optical table uses a 1550nm laser as the source. This laser is propagated through the ATS which imprints a scaled version of the turbulence profile into its phase. A FSM is used to compensate for the overall tip and tilt of the waverfront. The respective DM then applies a high-order correction to the wavefront. Once reflected off the DM the beam is sent to a SRI-WFS that directly measures the phase of the beam [5]. Figure 1 shows the optical layout of the table. The two DM's are placed conjugate to the pupil and the WFS, meaning they see the same wavefront as is in the entrance aperture (pupil) at the telescope.

For this particular experiment we have also placed a moveable optical trombone in the optical path to allow for the variation of the path length. This allows the user to adjust the scintillation in the system while keeping r_0 constant.

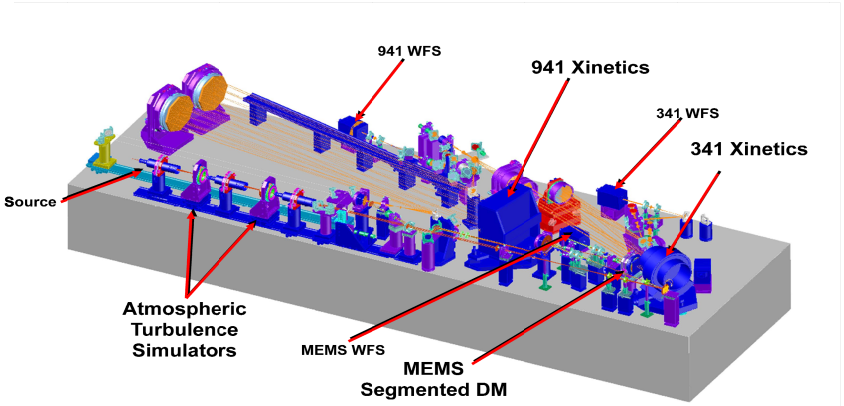

Figure 1 Optical layout of the optical table in the ASALT lab [6].

2.2 The deformable mirrors

The continuous face sheet DM is a Xinetics with 941 actuators arranged in a hexagonal array, of which 31x31 actuators are used for this particular experiment. This particular DM has an 8µm throw, a pixel pitch of 9mm and a fill factor of 100%. This DM uses 940W of power, has a volume of 0.43m^3 and weighs approximately 50kg.

The second DM used in the ASALT lab is a Boston Micromachines MEMS segmented device with 1024 actuators, a pixel pitch of 300µm and a fill factor of 98%. Mechanically, the power consumption of the MEMS is approximately 40W with a volume of 0.014m^3 and a weight of less than 5kg. The MEMS DM has an actuator throw of 1.5 µm. The MEMS device has 32x32 actuators with 30x30 actuators in use, making direct comparison to the Xinetics DM possible.

2.3 Control interface

The control interface consists of multiple computers that interface with different pieces of hardware on the table. Separate computers control each DM, scoring camera, WFS, etc. The main console, shown in Figure 2, controls all of the systems. This console consists of specific modules that merge both hardware control and processing algorithms. This console is highly flexible allowing the user to specify multiple aspects of the optics table. It is here where a specific real time reconstructor (RTR) is implemented, WFS reference files can be specified, phase wheel speeds can be adjusted, DM controls are set, etc. A specific console is designed for each experiment and data run conducted in the ASALT lab.

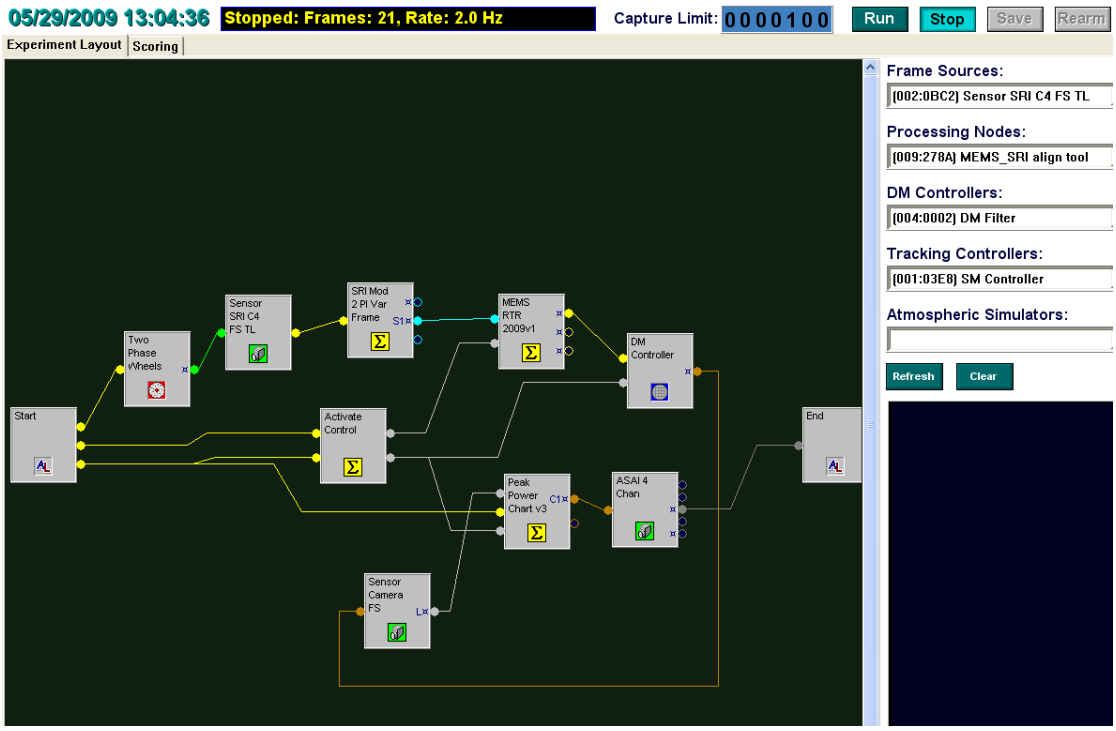

Figure 2 Screen shot of the control interface used in the ASALT lab.

2.4 Parameter set

The goal of this effort is to compare the two DM's in various turbulent regimes. A parameter set was chosen to interrogate the performance differences in weak, moderate and strong turbulence. For each turbulence case the optical trombone was used to keep r_0 constant while varying Rytov. Table 1 details each turbulence case. Note all parameter sets are scaled to a 1.5m aperture, at a 1kHz frame rate, and a constant Greenwood frequency.

r_0 (cm)	f_g (Hz)	Rytov					
9.70	33.8	0.31	0.37	0.44	0.50	0.57	0.63
7.13	33.8	0.50	0.62	0.72	0.83	0.93	1.03
5.00	33.8	1.07	1.26	1.46	1.64	1.89	2.00

Table 1 Parameter set used for the MAO experiments.

The parameter set in Table 1 demonstrates results in a wide range of atmospheric turbulence and scintillation. A second parameter set was also investigated focusing on increasing the scintillation while keeping r_0 constant. Table 2 details the second parameter set used.

r_0 (cm)	f_g (Hz)	Rytov										
7.13	33.8	0.50	0.62	0.72	0.83	0.93	1.03	1.13	1.22	1.32	1.41	1.51

Table 2 Second parameter set used for the MAO experiments.

3. THE CONTROL SYSTEM

3.1 Real time reconstructor

The SRI-WFS measures the phase of the beam in mod 2π space. This phase information needs to be converted to a functional form that the DM can use; this process is called reconstructing the wavefront. The algorithm that does this is called the reconstructor. The type of reconstructor used depends upon the type of DM being used, for example a continuous face sheet DM responds in a small zone around the actuators whereas a piston or tilt only DM respond to modal commands[6]. Figure 3 shows a block diagram indicating where the reconstructor fits into the AO system's control architecture.

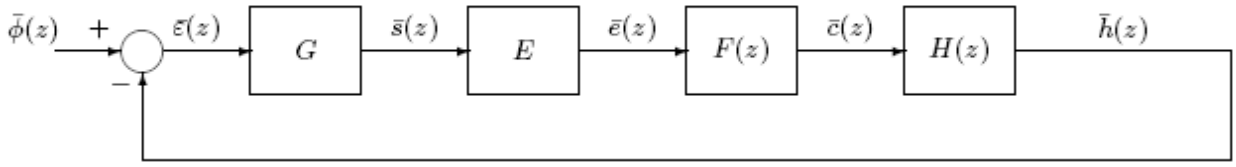

Figure 3 General model for the control loop of an adaptive optics system[7].

$\bar{\phi}(z)$ is the vector of phase disturbances at the actuator coordinates

$\bar{\varepsilon}(z)$ is the vector of phase errors at the actuator coordinates

$\bar{s}(z)$ is the vector of WFS gradient measurements

$\bar{e}(z)$ is the vector of phase errors after reconstruction

$\bar{c}(z)$ is the vector of commands applied to the DM

$\bar{h}(z)$ is the actual position of the actuators integrated over a measurement period

G is the influence function matrix

E is the reconstructor, taken to be the pseudo-inverse of $G, [\mathrm{E}] = (G^T G)^{-1} G^T$

$F(z)$ is the digital filter operator

$H(z)$ is the digital filter operator describing the impact of DM commands on integrated measurements on the WFS

The definition of the reconstructor, *E*, is the pseudo-inverse of the influence function matrix, *G*[7]. This is the conventional procedure for finding the reconstruction matrix in most adaptive optics systems. Here we will compare three different reconstructors, one for the Xinetics and two for the MEMS.

3.2 Methodology

We began by establishing baseline performance of the conventional AO system, i.e. the Xinetics DM with a least squares reconstructor for the initial comparisons. Both the Xinetics DM and the MEMS were driven by the same RTR. Also implemented was a MEMS specific RTR. The MEMS RTR uses the 2π modulo phase to create commands for the MEMS without unwrapping the phase first. The MEMS RTR shifts and scales the 2π modulo phase given to be in the range of –π to π. The next step subtracts a WFS reference if one is supplied. The difference of the 2π modulo phase and the WFS reference is taken in exponential space to keep the result in 2π modulo space. The real and imaginary components of the results are then used to calculate the reconstructed phase in the range –π to π [8].

In order to do a comprehensive comparison between the two DM's one needs to determine what parameters are important to study. For this research it was decided to concentrate on piston removal. The MEMS RTR estimates the piston in the current phase. This is done by averaging the real and imaginary components of all the points separately in phasor space. The averaged real and imaginary components are then converted into a magnitude of the averaged piston,

$-\pi$ to π. This RTR takes as inputs what WFS reference we use, the "leak" and servo gains (a and b respectively) and whether or not to implement the piston and tilt removal.

Three MEMS modules were designed to compare against a conventional adaptive optics (CAO) system. Each module is a control layout that combines both hardware control and processing algorithms. The first two modules are driven by the MEMS specific RTR, one allows for piston removal and one does not. The former takes the wrapped 2π phase and corrects for piston and sends the residual phase to the MEMS DM. The latter takes the wrapped 2π phase given from the SRI and sends it directly to the MEMS DM without removing piston first.

A third module that treats the MEMS as a continuous face sheet DM is also used. This module uses a conventional RTR that unwraps the phase using a least squares approximation. Tilt and piston are then approximated, and the tilt information is sent to the FSM for correction and the residual phase is then sent to the MEMS DM.

3.3 Data collection

A complete data set includes calibrations frames and frames taken using the above described modules. For each data set 12 different data runs where taken. Table 3 lists, in the order in which they were taken, each data run that is required to make a complete data set.

1.) Scintillation no turbulence (NT)	7.) CAO with turbulence
2.) Dark frame	8.) MEMS continuous_with turbulence
3.) CAO_NT	9.) MEMS w/o piston removal_ with turbulence
4.) MEMS continuous_NT	10.) MEMS with piston removal_with turbulence
5.) MEMS w/o piston removal_NT	11.) Scintillation_with turbulence
6.) MEMS with piston removal_NT	12.) Open loop

Table 3 List of the control modules used to compare the 941 with the MEMS.

This format was followed for each data set. For each r_0 value the above 12 data frames were taken for the 6 Rytov values outlined in Tables 1 and 2. The non-turbulent cases were taken with the laser beam going through the center of the phase wheels where there is no phase imprinted.

4. RESULTS AND DISCUSSION

Here we present the results of the data runs conducted in the ASALT lab.

4.1Results

As stated, we initially used an RTR with a least squares reconstructor to drive both DM's. Figure 4 shows a plot of Strehl versus r_0 for this particular data run.

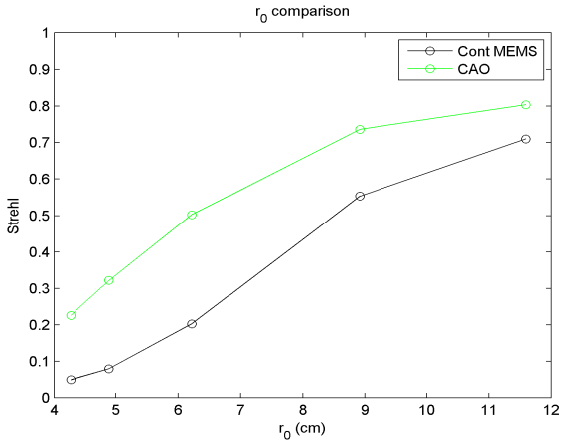

Figure 4 Strehl versus r0 for both the 941 and the MEMS using a traditional RTR.

This plot shows the MEMS AO system underperforming the conventional AO for all values of r_0. This performance differential was the motivation for the ASALT lab to look more carefully at the RTR used

Figure 5 shows an intermediate result from which the remainder of the analysis rests. The goal is to compare performance to a system that is known to perform well under certain atmospheric conditions. Figure 5 plots instantaneous Strehl versus frame number for an r_0 of 9.70cm and a Rytov of 0.50. The horizontal axis shows frame number, i.e. time, and the vertical axis shows bucket Strehl (power deposited at the target). This type of analysis shows the stability of the mean power over time indicating how well the DM performs as a function of how long the loop is closed.
The CAO plot (blue) serves as a baseline for all the other plots. The MEMS specific control modules are shown for piston removal in light blue, no piston removal in red, and the MEMS as a continuous face sheet in green along with open loop data (magenta).

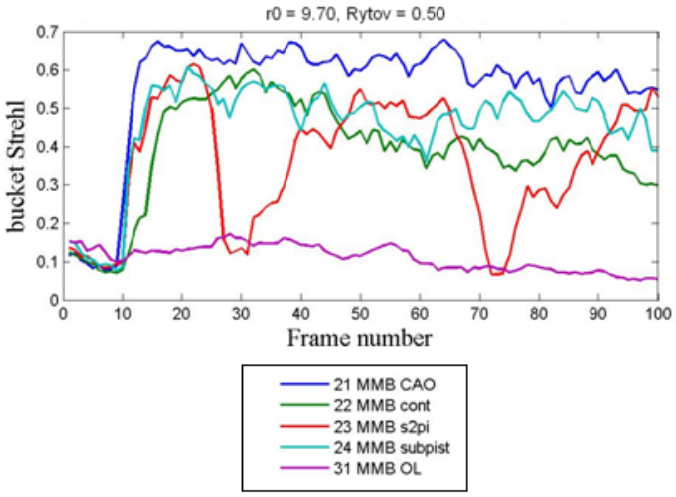

Figure 5 Plot of Strehl versus frame number for an r_0 of 9.70cm.

As can be seen here the conventional adaptive optics system is consistently outperforming the other MEMS specific modules. Also it can be seen that the non piston removal module (red) is showing some anomalies. The performance of this module appears to be oscillating in Strehl. This performance degradation is currently being investigated.

As described, data was taken in several different turbulent regimes. Figure 6 shows a plot of bucket Strehl versus frame number for an r_0 of 9.70, 7.13, and 5.00cm respectively. Again the horizontal axis represent frame number (time) and the vertical axis is bucket Strehl. For each r_0 value there were six corresponding Rytov values ranging from low to high.

Shown are the two extreme Rytov values for each r_0. The top row shows a weak turbulence regime with low and moderate scintillation values. The middle row plots an intermediate turbulence regime again moderate to high scintillation values, whereas the bottom row plots the deep turbulence regime with very high scintillation values.

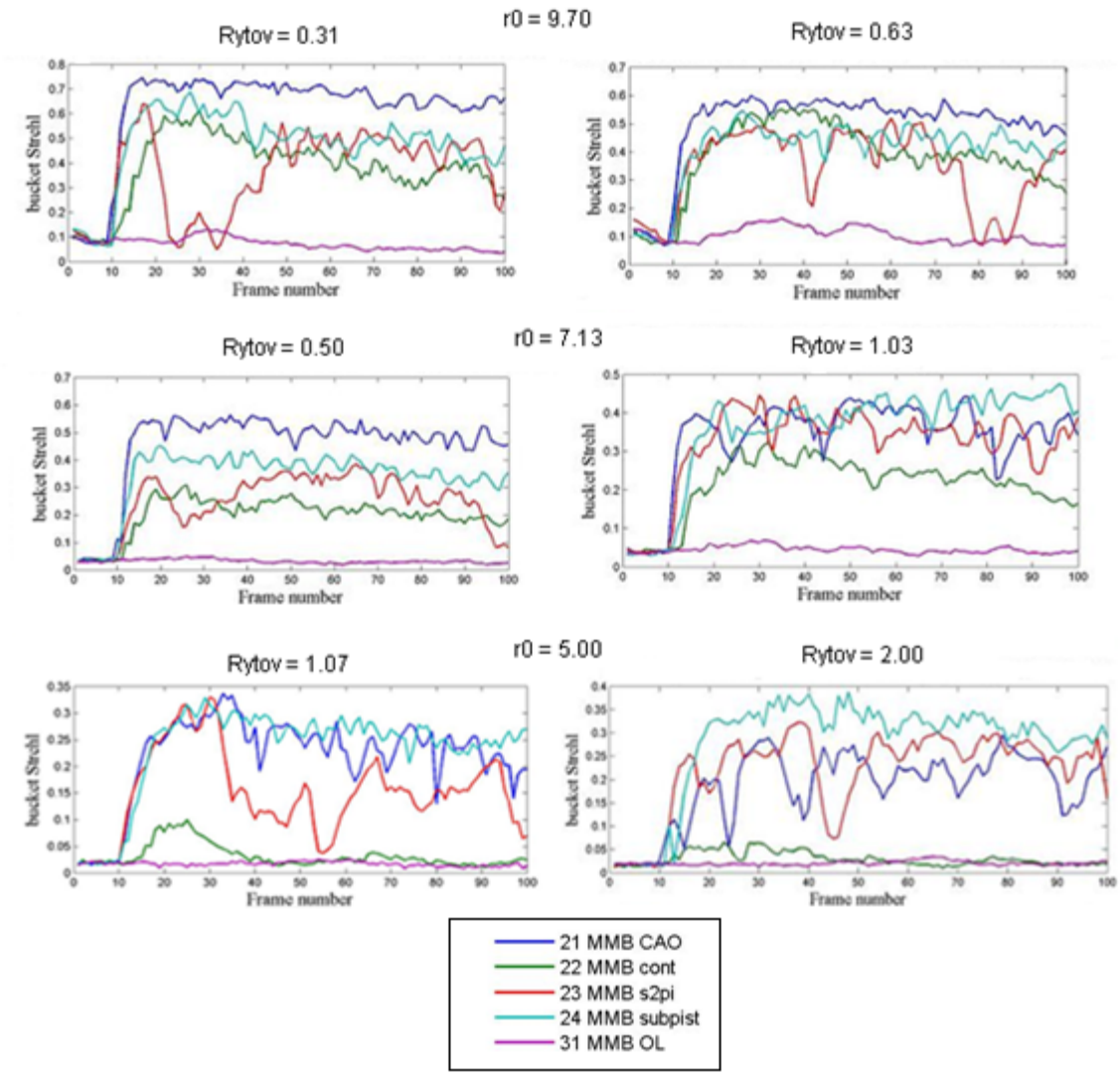

Figure 6 Plots of bucket Strehl versus frame number for three different r0 values and increasing Rytov.

It is consistently seen that the MEMS piston removal module (light blue) outperforms the MEMS non piston removal module (red) in every case. The third module (green) shows the MEMS being controlled with the same information as a continuous face sheet DM. Both the non piston removal and the MEMS continuous module are not performing as expected. The MEMS continuous algorithm has an issue with the function that reads in commands from the DM. This problem stems from the fact that in monochromatic light the MEMS essentially has infinite throw and the algorithm is not accounting for that; this gets dramatically worse as the turbulence increases. This causes the continuous module to degrade in performance the longer the loop is closed. Both modules are in process of being analyzed and retested.

The top row of Figure 6 (r_0 = 9.70) shows as Rytov increases the performance of both the MEMS and the conventional AO begins to slightly degrade with the conventional AO always outperforming the MEMS DM. This is expected since in weak turbulence the presence of rotational fields is low. The plots in the middle row show the same for a moderate turbulent regime with an r_0 of 7.13. Here we see the performance of both systems degrading slightly but, in this case, as Rytov increases the MEMS begins to outperform the 941. Here the MEMS performance is staying fairly constant as

Rytov increases whereas the performance for the 941 is degrading. Finally the bottom row of plots shows the deep turbulence regime with r_0 of 5.00cm. It is this regime where the MEMS excel. Here the 941's performance is degrading rapidly whereas the MEMS is showing steady performance. In this case the MEMS is outperforming the 941 for every Rytov value indicating a segmented device can be beneficial in stronger turbulence than a continuous face sheet DM. This would allow for observing at larger zenith angles through longer turbulence paths.

It is also advantageous to look at Strehl versus zenith angle (increase Rytov) because this determines how system performance degrades with increasing zenith angle. As the zenith angle increases, the scintillation increases. The plots in Figure 7 give the observer a better feel for how far off of zenith one can look before risking decreased AO performance. Figure 7 shows normalized bucket power versus zenith angle (hence increasing Rytov) for two r_0 values. The data shown here is the median of four data sets taken for each module.

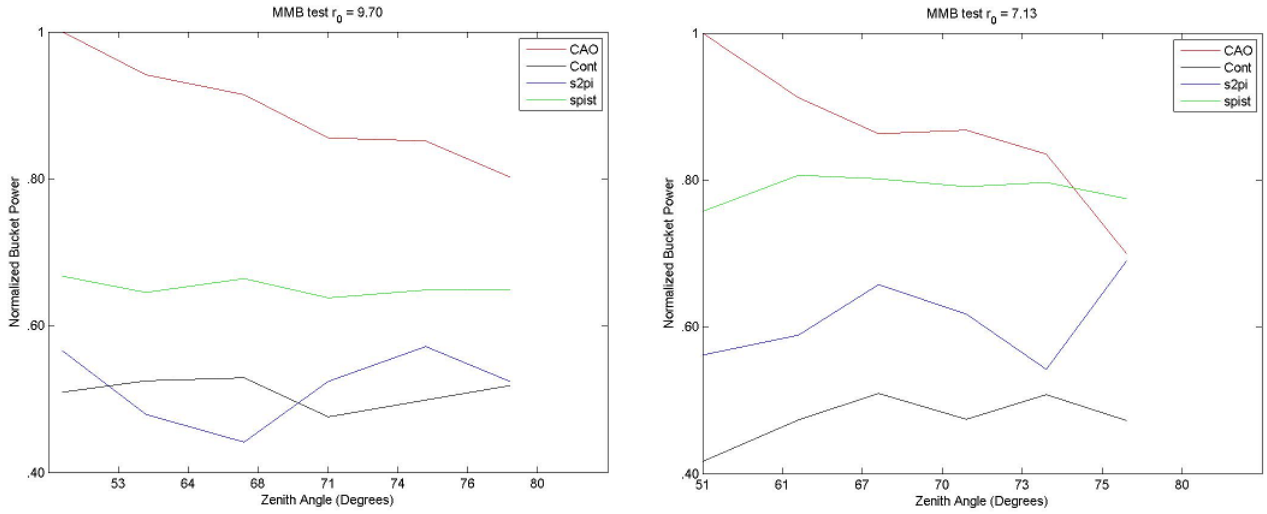

Figure 7 Normalized power versus zenith angle for two turbulent regimes.

In each individual plot one can see as the scintillation increases the performance of the CAO drops, where the MAO stays relatively constant. For r_0 of 9.70cm the CAO always outperforms the MAO, whereas for an r_0 of 7.13cm one can see a crossover at a Rytov of approximately 0.98. This crossover is investigated further in Figure 8 below. For an r_0 value of 5.00cm the MAO is always outperforming the CAO. As can be seen the MEMS piston removal routine actually begins to perform better as the turbulence increases.

Figure 8 studies in detail the crossover point at r_0 equal to 7.13cm. Here the values of Rytov were extended to correspond to a longer propagation length. The plot shows only the CAO (red) and the MEMS piston removal module (green). Again one can see that the performance of the CAO drops dramatically as the scintillation, i.e. zenith angle increases, whereas the performance of the MAO drops only slightly at high zenith angles indicating that a MAO system is better suited for moderate to high r_0 and high Rytov values.

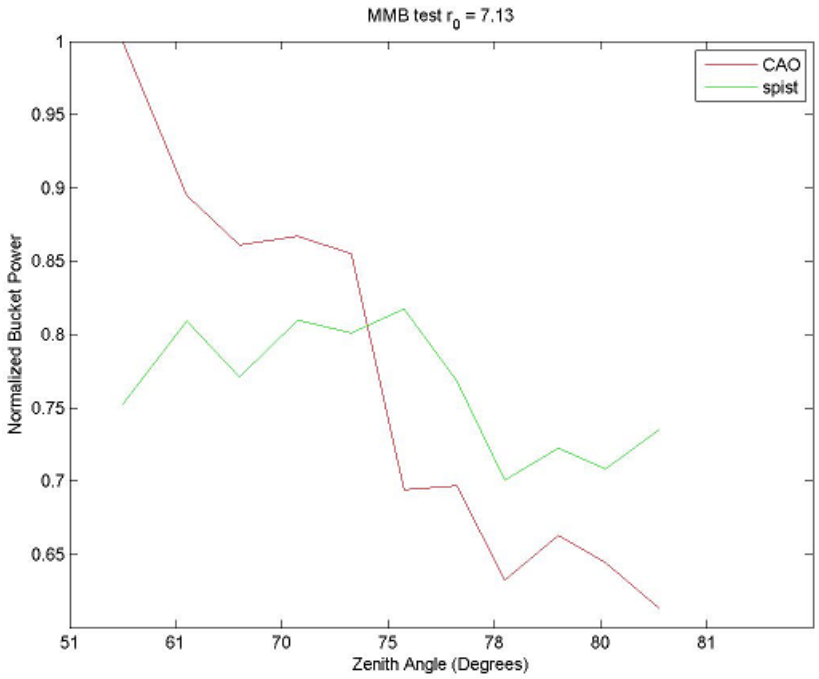

Figure 8 Normalized power versus zenith angle for r_0 7.13 through extended Rytov values.

4.2 Discussion and conclusion

The purpose of this experiment was to investigate the performance of two different types of DM's in various turbulence regimes pertinent to the astronomical community. A MEMS segmented DM was implemented into our existing AO testbed and closed loop operations were demonstrated. Initial closed loop testing was achieved using a traditional RTR with a least squares reconstructor. The results from this initial testing led to the design of a MEMS specific RTR. Three modules using the Boston Micromachines segmented MEMS DM were tested against a 941 Xinetics DM. The results showed enhanced performance from the MEMS in deep turbulence and high scintillation. We have shown that overall the MEMS shows better stability in all turbulent regimes compared to the 941 and shows less of a drop in performance as the turbulence increases. Also the MEMS mean Strehl stays fairly constant throughout all turbulent regimes, whereas there is an obvious drop in Strehl when using the 941 DM.

A MEMS device is much smaller and consumes much less power than a conventional DM, and is also much more cost effective. Since the performance of the MEMS at least matches that of a conventional DM in weak turbulence and excels in deep turbulence it has the potential to be deployed on new platforms in the astronomical community. Having a much smaller AO system allows for gimbal mounting on the sides of astronomical telescopes, which saves space of having a separate room devoted to the AO system. This research has shown that the implementation of a MAO system would allow for observing at higher zenith angles (lower elevation angles) through deeper turbulence.

It should be noted these experiments were done in the lab with a monochromatic light source. In monochromatic light the MEMS has essentially infinite throw. In polychromatic light the MEMS has only one eighth the throw of the Xinetics DM. This effect is being investigated further.

The research being conducted in the ASALT is essential to the advancement of AO technology. The efforts of the ASALT lab have led to a better understanding of different types of DM's and how best they can be incorporated into a science program. Along with a better understanding of particular AO systems, research of this nature allows the ASALT lab to advance our knowledge on how to test and implement AO systems in a well controlled environment.

This page intentionally left blank.

DISTRIBUTION LIST

DTIC/OCP
8725 John J. Kingman Rd, Suite 0944
Ft Belvoir, VA 22060-6218 1 cy

AFRL/RVIL
Kirtland AFB, NM 87117-5776 2 cy

Dan Devany
Official Record Copy
AFRL/RDSEW 1 cy